IEEE Access
Multidisciplinary | Rapid Review | Open Access Journal

Received August 21, 2018, accepted September 18, 2018, date of publication September 24, 2018,
date of current version November 14, 2018.

Digital Object Identifier 10.1109/ACCESS.2018.2871691

A Quantum Image Representation Based on Bitplanes

HAI-SHENG LI[1], XIAO CHEN[1], HAIYING XIA[1], YAN LIANG[1], AND ZUOSHAN ZHOU[2]
[1]College of Electronic Engineering, Guangxi Normal University, Guilin 541004, China
[2]Teachers College for Vocational and Technical Education, Guangxi Normal University, Guilin 541004, China

Corresponding authors: Zuoshan Zhou (295271625@qq.com) and Hai-Sheng Li (lhs_ecjtu@126.com)

This work was supported in part by the National Natural Science Foundation of China under Grant 61462026, Grant 61762012, and Grant 61762014, in part by the Project of Guangxi Normal University under Grant 2016ZD008, and in part by the Guangxi Normal University Education Development Foundation under Grant EDF2016004.

ABSTRACT Quantum image representation plays an important role in quantum image processing. In this paper, a bitplane representation of quantum images (BRQI) is proposed, which uses (n+4) or (n+6) qubits to store a grayscale or RGB color image of 2^n pixels. Compared with a novel enhanced quantum representation (NEQR), and a novel quantum representation of color digital images (NCQI), the storage capacity of BRQI improves 16 times and 2^{18} times, respectively. Next, some quantum operations based on BRQI are proposed, these operations including complement of colors, reverse of bitplanes, and translation of bitplanes. Analyzed the implementation circuits of these operations, the result indicates that these operations based on BRQI have lower quantum cost than NEQR and NCQI. Furthermore, an image scrambling algorithm based on BRQI is presented by combining the above operations. Simulation experiments and performance analysis show that proposed scrambling algorithm is effective and efficient.

INDEX TERMS Quantum image representation, quantum computing, bitplane, quantum image scrambling.

I. INTRODUCTION

Quantum image processing (QuIP) has been a hotspot in the field of image research in recent years, which has two outstanding merits: (1) the unique computing performance of quantum coherence, entanglement and superposition [1], and (2) quantum storage capacity increasing exponentially. Quantum image representation (QIR) is the foundation of quantum image processing. Many researches focus on the study of quantum image representation [2]–[16]. Some QIRs tore the color information using amplitudes of quantum states, such as Quantum Lattice [2], [3], a flexible representation of quantum images (FRQI) [4], a new quantum RGB multi-channel representation (MCQI) [5], and a normal arbitrary superposition state (NASS) representing an image [8]. These QIRs have displayed the enormous storage capacity of QuIP. For instance, FRQI stores a $2^n \times 2^n$ grayscale image using 2n+1 qubits. Furthermore, NASS stores a $2^n \times 2^n$ color image only using 2n qubits. However, these QIRs are difficult to retrieve accurately images from quantum systems using the low number of quantum measurement. For the convenience to retrieve accurately images, some QIRs store color information using basis states. For instance, a novel enhanced quantum representation (NEQR) [12], improved NEQR (INEQR) [13] and a generalized model of NEQR (GNEQR) [14] use 2n+8 qubits to store a $2^n \times 2^n$ grayscale image. A novel quantum representation of color digital images (NCQI) [15], and GNEQR stores a $2^n \times 2^n$ RGB color image using a 2n+24 qubits. Comparing NASS with NCQI, we discover the storage capacity of NASS is 2^{24} times of that of NCQI. In order to improve the storage capacity of QIRs which stores color information using basis states, the appropriate method of QIR is needed.

In addition, many quantum algorithms emerge continually, and these algorithms include quantum geometric transformation [17], quantum search algorithms [18], and quantum encryption [19]. Image scrambling is an important method of image encryption. Arnold transform [20], Hilbert scrambling, and bitplane scrambling are used to implemented quantum image encryption [21]–[23].

In order to improve the storage capacity of QIRs which stores color information using basis states, this paper proposes a bitplane representation of quantum images (BRQI), which can represent a grayscale or RGB color image of $2^n \times 2^n$ only using (2n+4) or (2n+6) qubits. Next, we

propose some quantum operations and a bitplane scrambling algorithm based on BRQI. Simulation experiments show the proposed algorithm is effective.

II. BACKGROUND

In the section, for clarity, we introduce some quantum gates and GNEQR, which have been described in [14].

A. QUANTUM GATES

Computational basis states $|0\rangle$, $|1\rangle$, and their dual states $\langle 0|$, $\langle 1|$ can be expressed as

$$|0\rangle = \begin{bmatrix} 1 \\ 0 \end{bmatrix}, \quad |1\rangle = \begin{bmatrix} 0 \\ 1 \end{bmatrix}, \quad \langle 0| = \begin{bmatrix} 1 & 0 \end{bmatrix}, \quad \langle 1| = \begin{bmatrix} 0 & 1 \end{bmatrix}. \tag{1}$$

Suppose that $|k\rangle$ is a basis state in a 2^n dimensional Hilbert space for $k = 0, 1, \cdots, 2^n - 1$, the state $|k\rangle$ and its dual state $\langle k|$ are

$$\begin{cases} |k\rangle = |k_{n-1}\rangle \otimes |k_{n-2}\rangle \otimes \ldots \otimes |k_0\rangle, \\ \langle k| = \langle k_{n-1}| \otimes \langle k_{n-2}| \otimes \ldots \otimes \langle k_0|, \end{cases} \tag{2}$$

where $k = \sum_{j=0}^{n-1} k_j \times 2^j$, $k_0, k_1, \ldots, k_{n-1} \in \{0, 1\}$, and $\otimes$ is the symbol of tensor product. We often use the abbreviated notations $|k_{n-1}\rangle |k_{n-2}\rangle \cdots |k_0\rangle$ or $|k_{n-1}k_{n-2}\ldots k_0\rangle$ for the tensor product $|k_{n-1}\rangle \otimes |k_{n-2}\rangle \otimes \ldots \otimes |k_0\rangle$.

A unitary gate corresponds to a unitary matrix U. The identity (I), Hadamard (H), Pauli-X (X), and $R_x(\arctan\sqrt{2})$ gates are four specific examples of the U gate, and their corresponding matrices are

$$I = \begin{bmatrix} 10 \\ 01 \end{bmatrix}, \quad X = \begin{bmatrix} 01 \\ 10 \end{bmatrix}, \quad H = \frac{\sqrt{2}}{2}\begin{bmatrix} 11 \\ 1-1 \end{bmatrix}, \quad R_x(\theta) = \begin{bmatrix} \cos\theta & \sin\theta \\ \sin\theta & -\cos\theta \end{bmatrix}, \tag{3}$$

where $\theta = \arctan\sqrt{2}$.

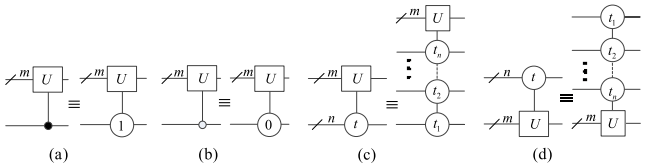

FIGURE 1. Notations of controlled-U gates. (a) $V_1^1(U)$. (b) $V_1^0(U)$. (c) $V_n^t(U)$. (d) $C_n^t(U)$. In (a) and (b), the numbers 1 and 0 can be replaced by black and white points on control qubits. In (c) and (d), $t_n \ldots t_2 t_1$ is the binary expansion of integer t, i.e., $t = \sum_{i=1}^{n} t_i \times 2^{i-1}$.

There are some controlled gates shown in Fig.1, where U is a gate of m qubits. When $U = X$, the controlled-U gate is also called as controlled-NOT (CNOT) gate shown in Fig.2.

B. INTRODUCTION OF GNEQR

Synthesizing NEQR, INEQR and NCQI, the literature [14] proposes a generalized model of NEQR (GNEQR), which is described as follows.

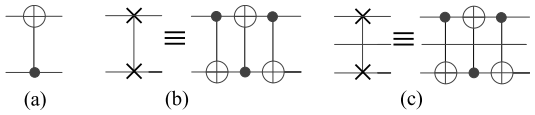

FIGURE 2. Three examples of controlled-U gates. (a) CNOT gate $V_1^1(X)$. (b) Swap gate. (c) Swap(3) gate (i.e., the Swap gate of 3 qubits).

A color set is defined as

$$\mathcal{C}_m = \{0, 1, \ldots, 2^m - 1\}, \tag{4}$$

where $\mathcal{C}_8$ and $\mathcal{C}_{24}$ are grayscale and RGB color sets, respectively. A basis state $|c\rangle$ with m qubits represents a color,

$$|c\rangle = |c_{m-1}\rangle |c_{m-2}\rangle \cdots |c_0\rangle = |c_{m-1}c_{m-2}\ldots c_0\rangle, \tag{5}$$

where $c_{m-1}c_{m-2}\ldots c_0$ is the binary expansion of the integer c.

When $c \in \mathcal{C}_8$ or $c \in \mathcal{C}_{24}$, $|c\rangle$ corresponds to a gray scale c or a RGB color (r, g, b), where $r = c_{23}c_{22}\ldots c_{16}$, $g = c_{15}c_{14}\ldots c_8$ and $b = c_7c_6\ldots c_0$.

GNEQR is defined as follows,

$$|\Psi_m\rangle = \frac{1}{\sqrt{2^n}} \sum_{x=0}^{2^{n-k}-1} \sum_{y=0}^{2^k-1} |f(x,y)\rangle |x\rangle |y\rangle, \tag{6}$$

where $|x\rangle = |i_{n-1}\ldots i_k\rangle$ and $|y\rangle = |i_{k-1}\ldots i_0\rangle$ are the X-axis and Y-axis of an image, and $i_0, \ldots i_k, \ldots, i_{n-1} \in \{0, 1\}$. Here, $|f(x,y)\rangle$ denotes the color of the pixel on the coordinate (x, y), $f(x,y) \in \mathcal{C}_m$. Therefore, $|\Psi_8\rangle$ and $|\Psi_{24}\rangle$ represent grayscale and color images of $2^{n-k} \times 2^k$, respectively.

For instance, the following GNEQR

$$\begin{aligned} |\Psi_8\rangle = \frac{1}{\sqrt{2^3}}(&|01100011\rangle |00\rangle |0\rangle + |01100100\rangle |00\rangle |1\rangle \\ &+ |01100001\rangle |01\rangle |0\rangle + |01100101\rangle |01\rangle |1\rangle \\ &+ |01100010\rangle |10\rangle |0\rangle + |01100100\rangle |10\rangle |1\rangle \\ &+ |01100101\rangle |11\rangle |0\rangle + |01100100\rangle |11\rangle |1\rangle) \end{aligned} \tag{7}$$

can store an image in Fig.3.

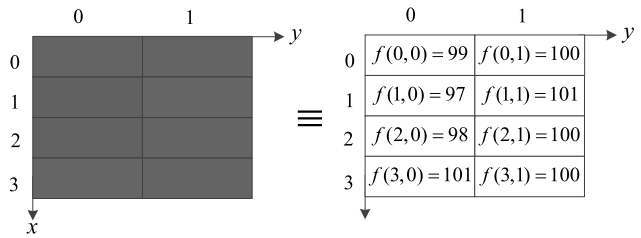

FIGURE 3. A 4 × 2 grayscale image.

III. A BITPLANE REPRESENTATION OF QUANTUM IMAGES (BRQI)

A. BRQI FOR GRAYSCALE IMAGES

A gray scale consists of 8 binary bits, so a grayscale image can be decomposed into 8 binary images (i.e., 8 bitplanes)

FIGURE 4. Bitplanes of a grayscale image.

shown in Fig.4. Each of bitplanes of a grayscale image can be represented using GNEQR,

$$\left|\Psi_m^j\right\rangle=\frac{1}{\sqrt{2^n}}\sum_{x=0}^{2^{n-k}-1}\sum_{y=0}^{2^k-1}|g(x,y)\rangle\,|x\rangle\,|y\rangle, \tag{8}$$

where j denotes the j-th bitplane, $j = 0, 1, \ldots, 7$, $m = 1$, $g(x, y) \in \mathcal{C}_1 = \{0, 1\}$.

For instance, the least significant bit (LSB) of the image in Fig.4 can be stored in

$$\begin{aligned}\left|\Psi_1^0\right\rangle = \frac{1}{\sqrt{2^3}}(&|1\rangle\,|00\rangle\,|0\rangle+|0\rangle\,|00\rangle\,|1\rangle+|1\rangle\,|01\rangle\,|0\rangle\\&+|1\rangle\,|01\rangle\,|1\rangle+|0\rangle\,|10\rangle\,|0\rangle+|0\rangle\,|10\rangle\,|1\rangle\\&+|1\rangle\,|11\rangle\,|0\rangle+|0\rangle\,|11\rangle\,|1\rangle).\end{aligned} \tag{9}$$

To represent the 8 bitplanes using a state, we define BRQI as follows, which consists of 8 GNEQR states in (8),

$$\begin{aligned}\left|\Psi_B^8\right\rangle &= \frac{1}{\sqrt{2^3}}\sum_{l=0}^{2^3-1}\left|\Psi_m^l\right\rangle|l\rangle\\&=\frac{1}{\sqrt{2^{n+3}}}\sum_{l=0}^{2^3-1}\sum_{x=0}^{2^{n-k}-1}\sum_{y=0}^{2^k-1}|g(x,y)\rangle\,|x\rangle\,|y\rangle\,|l\rangle\,,\end{aligned} \tag{10}$$

where $g(x, y) \in \mathcal{C}_1 = \{0, 1\}$, and l denotes the l-th bitplane.

From (10), we conclude that BRQI uses only qubits to represent a grayscale image. Compared to GNEQR in (8), its storage capacity improves 16 times.

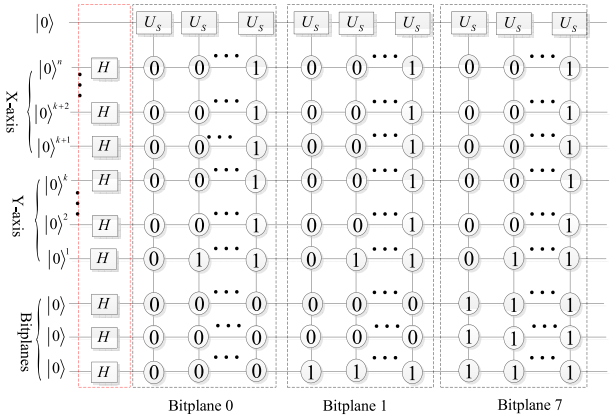

FIGURE 5. The implementation circuit of BRQI for grayscale images.

The implementation circuit of BRQI in (10) are designed in Fig.5, and its abbreviation circuits is shown in Fig.6.

In the Fig.5, the gate U_S is defined as

$$U_s = (g(x, y) \oplus 1)I + g(x, y)X, \tag{11}$$

where $\oplus$ is an exclusive-or operator. I.e., if $g(x, y) = 0$, $U_s = I$, otherwise, $U_s = X$.

The circuit in the red dashed box implements

$$\begin{aligned}&(I\otimes H^{\otimes n-k}\otimes H^{\otimes k}\otimes H^{\otimes 3})\,|0\rangle\,|0\rangle^{\otimes n-k}|0\rangle^{\otimes k}|0\rangle^{\otimes 3}\\&=\frac{1}{\sqrt{2^{n+3}}}\sum_{l=0}^{2^3-1}\sum_{x=0}^{2^{n-k}-1}\sum_{y=0}^{2^k-1}|0\rangle\,|x\rangle\,|y\rangle\,|l\rangle\,,\end{aligned} \tag{12}$$

where $H^{\otimes n}$ and $|0\rangle^{\otimes n}$ are the n fold tensor products of H and $|0\rangle$, respectively.

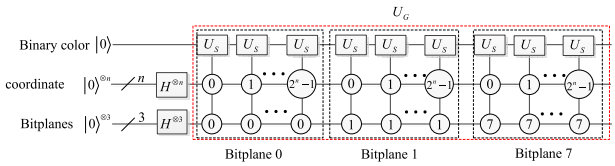

FIGURE 6. The abbreviation circuit of BRQI for grayscale images. The circuit of the red dashed box is symbolized as U_G.

The circuit in the dashed box bitplane j ($j = 0, 1, \ldots, 7$) stores the j-th bitplane in quantum systems. Therefore, the circuit U_G in Fig.6 implements

$$\frac{1}{\sqrt{2^{n+3}}}\sum_{l=0}^{2^3-1}\sum_{x=0}^{2^{n-k}-1}\sum_{y=0}^{2^k-1}|0\rangle\,|x\rangle\,|y\rangle\,|l\rangle\rightarrow\left|\Psi_B^8\right\rangle. \tag{13}$$

For instance, we can store the image in Fig.3 in quantum systems using the circuit in Fig.7.

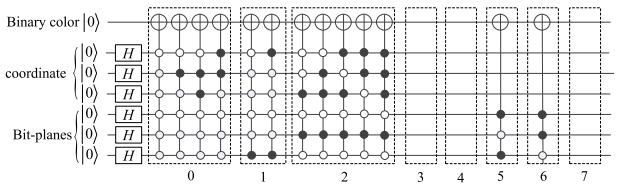

FIGURE 7. The implementation circuit of BRQI for grayscale images.

The circuit in dashed box l is the implementation circuit of the l-th bitplane $\left|\Psi_1^l\right\rangle$, where $l = 0, 1, \ldots, 7$. Since the pixel values of the 3rd, 4-th, and 7-th bitplanes are all zero, corresponding circuits do nothing. Furthermore, the pixel values of the 5-th and 6-th bitplanes are both one, then, their implementation circuits can be simplified, which are shown in the dashed boxes 5 and 6. The output of the circuit in Fig.7 is

$$\left|\Psi_B^8\right\rangle=\frac{1}{\sqrt{2^3}}\sum_{l=0}^{7}\left|\Psi_1^l\right\rangle|l\rangle, \tag{14}$$

where $|\Psi_1^0\rangle$ is shown in (9), and

$$\begin{cases} |\Psi_1^1\rangle = \frac{1}{\sqrt{2^3}}(|1\rangle|00\rangle|0\rangle + |0\rangle|00\rangle|1\rangle \\ \quad + |0\rangle|01\rangle|0\rangle + |0\rangle|01\rangle|1\rangle + |1\rangle|10\rangle|0\rangle \\ \quad + |0\rangle|10\rangle|1\rangle + |0\rangle|11\rangle|0\rangle + |0\rangle|11\rangle|1\rangle), \\ |\Psi_1^2\rangle = \frac{1}{\sqrt{2^3}}(|0\rangle|00\rangle|0\rangle + |1\rangle|00\rangle|1\rangle \\ \quad + |0\rangle|01\rangle|0\rangle + |1\rangle|01\rangle|1\rangle + |0\rangle|10\rangle|0\rangle \\ \quad + |1\rangle|10\rangle|1\rangle + |1\rangle|11\rangle|0\rangle + |1\rangle|11\rangle|1\rangle), \\ |\Psi_1^3\rangle = |\Psi_1^4\rangle = |\Psi_1^7\rangle = \frac{1}{\sqrt{2^3}}\sum_{x=0}^{3}\sum_{y=0}^{1}|0\rangle|x\rangle|y\rangle, \\ |\Psi_1^5\rangle = |\Psi_1^6\rangle = \frac{1}{\sqrt{2^3}}\sum_{x=0}^{3}\sum_{y=0}^{1}|1\rangle|x\rangle|y\rangle. \end{cases} \tag{15}$$

B. BRQI FOR RGB COLOR IMAGES

When $m = 24$, $|c\rangle$ in (5) can be rewritten as

$$\begin{aligned} |c\rangle &= |c_{23}\rangle|c_{22}\rangle\cdots|c_0\rangle \\ &= |c_{23}c_{22}\ldots c_{16}\rangle|c_{15}c_{14}\ldots c_8\rangle|c_7c_6\ldots c_0\rangle, \end{aligned} \tag{16}$$

i.e., a RGB color image can be decomposed into three grayscale images or 24 bitplanes.

Similarly with (10), three components of a RGB color image can be written as

$$\begin{cases} |\Psi_B^R\rangle = \frac{1}{\sqrt{2^{n+3}}}\sum_{l=0}^{2^3-1}\sum_{x=0}^{2^{n-k}-1}\sum_{y=0}^{2^k-1}|g_R(x,y)\rangle|x\rangle|y\rangle|l\rangle, \\ |\Psi_B^G\rangle = \frac{1}{\sqrt{2^{n+3}}}\sum_{l=0}^{2^3-1}\sum_{x=0}^{2^{n-k}-1}\sum_{y=0}^{2^k-1}|g_G(x,y)\rangle|x\rangle|y\rangle|l\rangle, \\ |\Psi_B^B\rangle = \frac{1}{\sqrt{2^{n+3}}}\sum_{l=0}^{2^3-1}\sum_{x=0}^{2^{n-k}-1}\sum_{y=0}^{2^k-1}|g_B(x,y)\rangle|x\rangle|y\rangle|l\rangle, \end{cases} \tag{17}$$

where $g_R(x,y), g_G(x,y), g_B(x,y) \in C_1 = \{0,1\}$.

Furthermore, BRQI for RGB color images can be defined as

$$|\Psi_B^{24}\rangle = \frac{1}{\sqrt{3}}(|\Psi_B^R\rangle|01\rangle + |\Psi_B^G\rangle|10\rangle + |\Psi_B^B\rangle|11\rangle). \tag{18}$$

The implementation circuit of $|\Psi_B^{24}\rangle$ is designed in Fig.8.

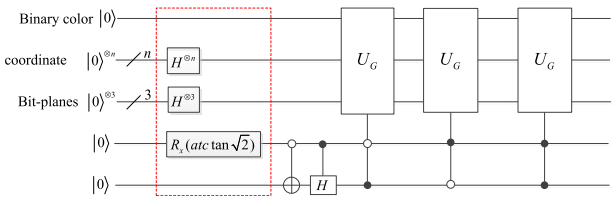

FIGURE 8. The implementation circuit of BRQI for RGB color images.

The circuit in the red dashed box in Fig.8 implements

$$\begin{aligned} &|0\rangle|0\rangle^{\otimes n-k}|0\rangle^{\otimes k}|0\rangle^{\otimes 3}|00\rangle \\ &\rightarrow \frac{1}{\sqrt{3\times 2^{n+3}}}\left(\sum_{l=0}^{2^3-1}\sum_{x=0}^{2^{n-k}-1}\sum_{y=0}^{2^k-1}|0\rangle|x\rangle|y\rangle|l\rangle|01\rangle\right. \\ &\quad + \sum_{l=0}^{2^3-1}\sum_{x=0}^{2^{n-k}-1}\sum_{y=0}^{2^k-1}|0\rangle|x\rangle|y\rangle|l\rangle|10\rangle \\ &\quad \left. + \sum_{l=0}^{2^3-1}\sum_{x=0}^{2^{n-k}-1}\sum_{y=0}^{2^k-1}|0\rangle|x\rangle|y\rangle|l\rangle|11\rangle\right). \end{aligned} \tag{19}$$

From (12) and (18), we obtain that the circuit in Fig.8 implements

$$|0\rangle|0\rangle^{\otimes n-k}|0\rangle^{\otimes k}|0\rangle^{\otimes 3}|00\rangle \rightarrow |\Psi_B^{24}\rangle. \tag{20}$$

C. IMAGE RETRIEVING

Quantum measurement is a unique way to retrieve classical information from a quantum state. A quantum state will collapse after measurement. Then it is impossible to get all information of a quantum superposition state with only one quantum measurement. Therefore a measurement process needs many identical quantum states [4]. We describe the measurement operation as below to retrieve image from BRQI.

To retrieving an image from BRQI $|\Psi_B^8\rangle$ in (10), we define an observable operator as

$$\begin{cases} M_1 = \sum_{i=0}^{2^{n+4}-1} e_i P_i, \\ P_i = |m\rangle|x\rangle|y\rangle|l\rangle\langle m|\langle x|\langle y|\langle l| = |i\rangle\langle i|, \end{cases} \tag{21}$$

where P_i is the projector onto the eigenspace of M_1 with eigenvalue e_i; $x_{n-k-1}\ldots x_1x_0$, $y_{k-1}\ldots y_1y_0$, $l_2l_1l_0$, and $mx_{n-k-1}\ldots x_1x_0y_{k-1}\ldots y_1y_0l_2l_1l_0$ are the binary expansions of integers x, y, l, and i, respectively.

Applying the observable operator M_1 to the state $|\Psi_B^8\rangle$ in (10), we get the result m_i with the probability

$$p(m_i) = \langle\Psi_B^8|P_i|\Psi_B^8\rangle = \frac{1}{2^{n+3}}, \tag{22}$$

Given that outcome m_i occurred, the state after the measurement is

$$\frac{P_i|\Psi_B^8\rangle}{\sqrt{p(i)}} = |m\rangle|x\rangle|y\rangle|l\rangle, \tag{23}$$

i.e., we obtain the color of the pixel on coordinate (x,y) in the l-th bitplane with the probability $(1/2^{n+3})$.

Similarly, a collection of quantum measurement operators

$$M_2 = I^{\otimes n+4} \otimes \{|00\rangle\langle 00|, |01\rangle\langle 01|, |10\rangle\langle 10|, |11\rangle\langle 11|\} \tag{24}$$

are applied to the state $|\Psi_B^{24}\rangle$ in (18), which collapses into one of $\{|\Psi_B^R\rangle, |\Psi_B^G\rangle, |\Psi_B^B\rangle\}$. Given that outcome $|\Psi_B^R\rangle$ occurred, next, we can retrieve image from $|\Psi_B^R\rangle$ using the observable operator in (21).

D. SIMULATION VERIFICATION OF IMPLEMENTATION CIRCUITS

Postulate 3 (i.e., evolution postulate) of quantum mechanics describes that the evolution of a closed quantum system is described by a unitary transformation, therefore quantum operations can be simulated using unitary matrixes. Single qubit and CNOT gates can be used to implement an arbitrary unitary operation on n qubits [1], so we describe that how to calculate the matrices of controlled gates.

Two controlled-U gates in Fig.1 (c) and (d) can be calculated by

$$\begin{cases} V_n^j(U) = (U \otimes |j\rangle\langle j|) + \sum_{i=0, i\neq j}^{2^n-1} (I^{\otimes m} \otimes (|i\rangle\langle i|)), \\ C_n^j(U) = (|j\rangle\langle j|) \otimes U + \sum_{i=0, i\neq j}^{2^n-1} ((|i\rangle\langle i|) \otimes I^{\otimes m}). \end{cases} \tag{25}$$

where U is a gate of m qubits.

For instance, by using (25), we obtain the matrices of the gates in Fig.2 (a) and (b) as follows,

$$V_1^1(X) = \begin{bmatrix} 1 & 0 & 0 & 0 \\ 0 & 0 & 0 & 1 \\ 0 & 0 & 1 & 0 \\ 0 & 1 & 0 & 0 \end{bmatrix}, \quad Swap = \begin{bmatrix} 1 & 0 & 0 & 0 \\ 0 & 0 & 1 & 0 \\ 0 & 1 & 0 & 0 \\ 0 & 0 & 0 & 1 \end{bmatrix}. \tag{26}$$

As an example, the circuit in Fig.7 is used to verify the correctness of the implementation circuit of BRQI.

We calculate the vector of $\left|\Psi_B^8\right\rangle$ in (14) using (2),

$$\begin{aligned} V_8 = \frac{1}{8}[&0,0,1,1,1,0,0,1,1,1,0,1,1,0,0,1,0,1,1,\\ &1,1,0,0,1,0,1,0,1,1,0,0,1,1,0,1,1,1,0,0,1,1,\\ &1,0,1,1,0,0,1,0,1,0,1,1,0,0,1,1,1,0,1,1,0,0,\\ &1,1,1,0,0,0,1,1,0,0,0,1,0,0,1,1,0,1,0,0,0,0,\\ &1,1,0,1,0,1,0,0,1,1,0,0,1,0,0,0,1,1,0,0,0,1,\\ &0,0,1,1,0,1,0,1,0,0,1,1,0,\ 0,0,1,0,0,1,1,0]^T, \end{aligned} \tag{27}$$

where $[\ ]^T$ is a matrix transpose operation.

Using (25), we calculate the matrix of the circuit in Fig.7,

$$U_8 = \left(\prod_{i=0}^{7} V_i\right)(I \otimes H^{\otimes 6}), \tag{28}$$

where V_i is the matrix of the circuit in the i-th dashed box, and

$$\begin{cases} V_0 = C_6^{48}(X)C_6^{24}(X)C_6^{16}(X)C_6^{0}(X), \\ V_1 = C_6^{33}(X)C_6^{1}(X), \\ V_2 = C_6^{58}(X)C_6^{50}(X)C_6^{42}(X)C_6^{26}(X)C_6^{10}(X), \\ V_5 = C_3^5(X \otimes I^{\otimes 3}), \\ V_6 = C_3^6(X \otimes I^{\otimes 3}), \\ V_3 = V_4 = V_7 = I^{\otimes 7}. \end{cases}$$

The initial state $|0\rangle^{\otimes 7}$ corresponds to the vector $[1,0,\ldots,0]^T$ of size 128×1, then, we obtain a vector $V = U_8[1,0,\ldots,0]^T$ using Matlab. Comparing V with V_8 in (27), we can verify the correctness of the implementation circuit of BRQI.

E. COMPARISON OF QIRS

Table 1 compares eight QIRs for grayscale images (GI) or RGB color images (CI). It shows that FRQI, NASS and MCQI require fewer qubits than others. Since their pix encoding is probability amplitude, they are more difficult on image retrieve. When the color information of pixels is encoded by basis states, the storage capacity of BRQI improves 16 times for grayscale images, and 2^{18} times for RGB color images.

TABLE 1. comparison of QIRS for an image of 2^{2n} pixels.

QIR	Qubits (GI)	Qubits (CI)	Image size	Pixel encoding
FRQI [4]	2n+1	-	$2^{2n-k} \times 2^k$	Amplitude
NASS [8]	2n	2n	$2^{2n-k} \times 2^k$	Amplitude
MCQI[5]	-	2n+3	$2^{2n-k} \times 2^k$	Amplitude
NEQR[12]	2n+8	-	$2^n \times 2^n$	Basis states
INEQR[13]	2n+8	-	$2^{2n-k} \times 2^k$	Basis states
NCQI[15]	-	2n+24	$2^n \times 2^n$	Basis states
GNEQR[14]	2n+8	2n+24	$2^{2n-k} \times 2^k$	Basis states
BRQI	2n+4	2n+6	$2^{2n-k} \times 2^k$	Basis states

IV. QUANTUM IMAGE PROCESSING BASED ON BRQI

In the above section, we have described that how to calculate the vector of BRQI and matrices of circuits. Therefore, we design some operations based on BRQI, and use a 64×64 grayscale image as an example to verify the correctness of these operations. Simulation experiments are implemented in Matlab R2017a, windows 7, and 56GB RAM.

A. COMPLEMENT OPERATION OF COLORS

BRQI uses only one qubit to store the color information of an image, therefore, a NOT gate can implement color complement operations of the whole image of 2^n pixels, i.e., the complement operation is defined as

$$U_C = X \otimes I^{\otimes n+3}. \tag{29}$$

Applying U_C to the state $\left|\Psi_B^8\right\rangle$ in (10), we obtain

$$\begin{aligned} U_C\left|\Psi_B^8\right\rangle &= (X \otimes I^{\otimes n+3})\frac{1}{\sqrt{2^3}}\sum_{l=0}^{2^3-1}\left|\Psi_m^l\right\rangle|l\rangle \\ &= \frac{1}{\sqrt{2^{n+3}}}\sum_{l=0}^{2^3-1}\sum_{x=0}^{2^{n-k}-1}\sum_{y=0}^{2^k-1}|1-g(x,y)\rangle|x\rangle|y\rangle|l\rangle, \end{aligned} \tag{30}$$

which is implemented by the circuit in Fig.9 (a).

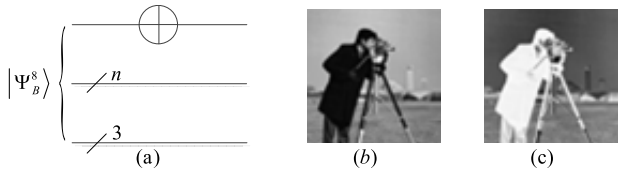

FIGURE 9. A complement operation based on BRQI. (a) The implementation circuit of U_C. (b) A 64 × 64 grayscale image. (c) The result of the complement operation.

Note: Suppose that a 128 × 128 grayscale image is stored in $|\Psi_B^8\rangle$, which is equivalent to a $2^{14} \times 1$ vector, we get a $2^{18} \times 2^{18}$ matrix of U_C using (29). Set the data type of elements in the matrix to single-precision real number, the matrix of U_C needs 256 GB RAM, which is too big for our computers, so we select only a 64 × 64 grayscale image as the example of simulation experiments.

B. REVERSE OPERATION OF BITPLANES

BRQI uses three qubits to store the bitplane information of an image, therefore, three NOT gates can implement reverse order of bitplanes of a grayscale image of 2^n pixels. The reverse operation of bitplanes is defined as

$$U_R = I^{\otimes n+1} \otimes X^{\otimes 3}. \tag{31}$$

Applying U_R to the state $|\Psi_B^8\rangle$ in (10), we have

$$\begin{aligned} U_R \left|\Psi_B^8\right\rangle &= (I^{\otimes n+1} \otimes X^{\otimes 3}) \frac{1}{\sqrt{2^3}} \sum_{l=0}^{2^3-1} \left|\Psi_m^l\right\rangle |l\rangle \\ &= \frac{1}{\sqrt{2^3}} \sum_{l=0}^{2^3-1} \left|\Psi_m^l\right\rangle |7-l\rangle , \end{aligned} \tag{32}$$

which is implemented by the circuit in Fig.10 (a). Simulation results are shown in Fig.10and Fig.11.

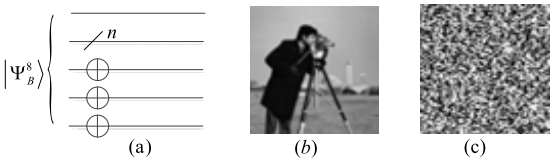

FIGURE 10. A reverse operation of bitplanes. (a) The implementation circuit of U_R. (b) A 64 × 64 grayscale image. (c) The result of the reverse operation.

From Fig.10, we infer that U_R can be regarded as an operation of image scrambling. However, the operation U_R can't transform the value of pixels in a bitplane. For instance, bitplanes of the image in Fig.10 (c) are shown in Fig.11.

C. OPERATION OF PIXEL INTERCHANGE AMONG BITPLANES

Each of pixels in a bitplane has only two gray scale, i.e., 0 and 1. Therefore, we use only two controlled Swap gates to implement the operation of pixel interchange among

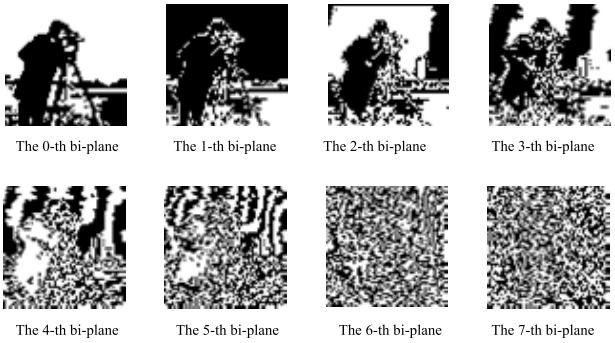

FIGURE 11. Bitplanes of the image in Fig.10 (c).

bitplanes, which is defined as

$$\begin{cases} U_I = C_1^0(U_0)C_1^1(U_1) = |0\rangle\langle 0| \otimes U_0 + |1\rangle\langle 1| \otimes U_1, \\ U_0 = I^{\otimes n+1} \otimes Swap, \\ U_1 = I^{\otimes n} \otimes Swap(3), \end{cases} \tag{33}$$

where $C_1^0(U_0)$, $C_1^1(U_1)$, Swap and Swap(3) gates are shown in Fig.1 and Fig.2, respectively.

FIGURE 12. The operation of pixel interchange. (a) The implementation circuit of U_I. (b) A 64 × 64 grayscale image. (c) The result of the pixel interchange operation.

The circuit of U_I is designed in Fig.12 (a) and implements

$$\begin{cases} |l_2 l_1 l_0\rangle \leftrightarrow |l_2 l_0 l_1\rangle , & \text{when } g(x,y) = 0, \\ |l_2 l_1 l_0\rangle \leftrightarrow |l_0 l_1 l_2\rangle , & \text{when } g(x,y) = 1, \end{cases} \tag{34}$$

where $|l_2 l_1 l_0\rangle$ is the encoding of the original image.

Applying U_I to the image in Fig.12(b), we obtain its simulation results in Fig.12 (c) and Fig.13.

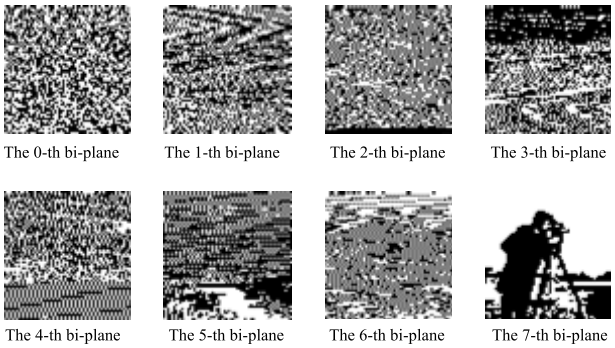

FIGURE 13. Bitplanes of the image in Fig.12 (c).

From (34) and Fig.13, we infer that the pixels in the 0-th and 7-th bitplanes remain unchanged.

D. TRANSLATION OPERATION OF BITPLANES

The translation operation of bitplanes is defined as

$$U_A = (I^{\otimes n+1} \otimes V_2^3(X))(I^{\otimes n+2} \otimes V_1^1(X))(I^{\otimes n+3} \otimes X), \quad (35)$$

where $V_2^3(X)$ and $V_1^1(X)$ are shown in Fig.1.

Applying U_A to the state $\left|\Psi_B^8\right\rangle$ in (10), we have

$$U_A \left|\Psi_B^8\right\rangle = \frac{1}{\sqrt{2^3}} \sum_{l=0}^{2^3-1} \left|\Psi_m^l\right\rangle |l-_8 1\rangle, \quad (36)$$

where $l-_8 1 = (l-1) \bmod 8$, and mod is a modulo operation.

The circuit and simulation result of U_A are shown in Fig.14 and Fig.15.

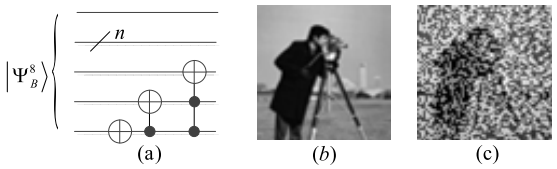

FIGURE 14. A translation of bitplanes. (a) The implementation circuit of U_A. (b) A 64 × 64 grayscale image. (c) The result of the translation.

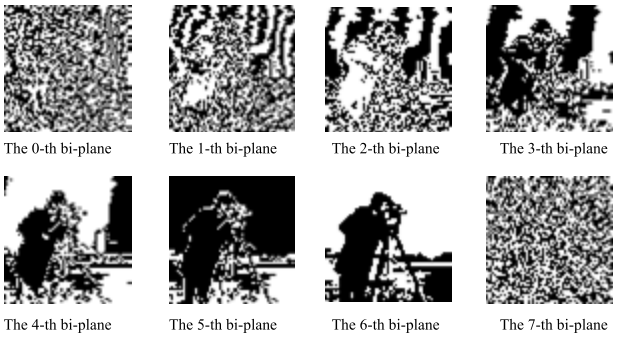

FIGURE 15. Bitplanes of the image in Fig.14.

Fig.15 shows that the operation U_A implements left translation of bitplanes.

E. THE ALGORITHM OF IMAGE SCRAMBLING BASED ON BRQI

Combining the above operations, we design the algorithm of image scrambling as follows,

$$U_S = U_R U_C U_I U_T, \quad (37)$$

which is implemented by the circuit in Fig.16 (a).

Applying the operation to four images in Fig.16(b) - (e) respectively, we obtain the transformed images shown in Fig.16 (f) - (i), bitplanes of which are shown in Fig.17.

Simulation results in Fig.16 and Fig.17 show that proposed algorithm of image scrambling is effective.

Set

$$\begin{cases} U_C^C = U_C \otimes I^{\otimes 2}, \\ U_R^C = U_R \otimes I^{\otimes 2}, \\ U_I^C = U_I \otimes I^{\otimes 2}, \\ U_T^C = U_T \otimes I^{\otimes 2}, \\ U_S^C = U_R^C U_C^C U_I^C U_T^C = U_S \otimes I^{\otimes 2}, \end{cases} \quad (38)$$

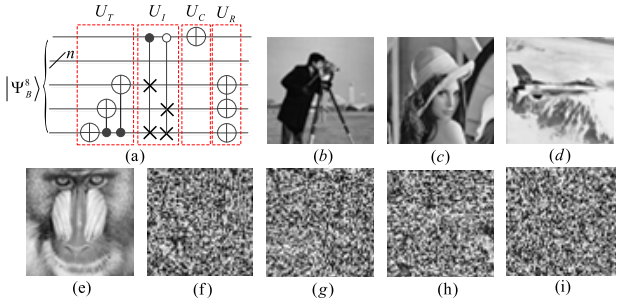

FIGURE 16. An image scrambling algorithm based on bitplanes. (a) The implementation circuit of the image scrambling. (b) Cman image. (c) Lena image. (d) Airplane image. (e) Baboon image. (f) Transformed Cman image. (g) Transformed Lena image. (h) Transformed Airplane image. (i) Transformed Baboon image.

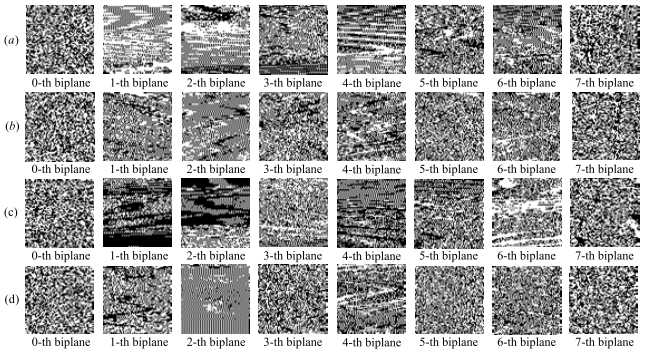

FIGURE 17. Bitplanes of the transformed images. (a) Bitplanes of the transformed Cman image. (b) Bitplanes of the transformed Lena image. (c) Bitplanes of the transformed Airplane image. (d) Bitplanes of the transformed Baboon image.

we have

$$\begin{cases} U_C^C \left|\Psi_B^{24}\right\rangle \\ = \frac{1}{\sqrt{3}}(U_C \left|\Psi_B^R\right\rangle |01\rangle + U_C \left|\Psi_B^G\right\rangle |10\rangle + U_C \left|\Psi_B^B\right\rangle |11\rangle), \\ U_R^C \left|\Psi_B^{24}\right\rangle \\ = \frac{1}{\sqrt{3}}(U_R \left|\Psi_B^R\right\rangle |01\rangle + U_R \left|\Psi_B^G\right\rangle |10\rangle + U_R \left|\Psi_B^B\right\rangle |11\rangle), \\ U_I^C \left|\Psi_B^{24}\right\rangle \\ = \frac{1}{\sqrt{3}}(U_I \left|\Psi_B^R\right\rangle |01\rangle + U_I \left|\Psi_B^G\right\rangle |10\rangle + U_I \left|\Psi_B^B\right\rangle |11\rangle), \\ U_T^C \left|\Psi_B^{24}\right\rangle \\ = \frac{1}{\sqrt{3}}(U_T \left|\Psi_B^R\right\rangle |01\rangle + U_T \left|\Psi_B^G\right\rangle |10\rangle + U_T \left|\Psi_B^B\right\rangle |11\rangle), \\ U_S^C \left|\Psi_B^{24}\right\rangle \\ = \frac{1}{\sqrt{3}}(U_S \left|\Psi_B^R\right\rangle |01\rangle + U_S \left|\Psi_B^G\right\rangle |10\rangle + U_S \left|\Psi_B^B\right\rangle |11\rangle), \end{cases} \quad (39)$$

where $\left|\Psi_B^{24}\right\rangle$ is BRQI for RGB color images (see (18)).

Therefore, U_C^C, U_R^C, U_I^C, U_T^C, and U_S^C are the complement, reverse, pixel interchange, translation, and image scrambling operations for RGB color images, respectively. Their circuits are designed in Fig.18.

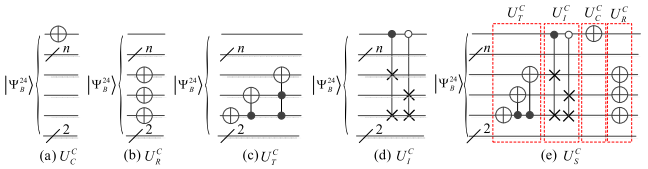

FIGURE 18. Operations based on BRQI for color images.

TABLE 2. The costs of some basic gates.

Gate	Cost
CNOT gate	1
Controlled Swap gate (i.e., Fredkin gate) [22]	5
Controlled NOT gate of 2 qubits (i.e., Toffoli gate) [1]	5
Swap gate	3
NOT gate	$\delta \ll 1$

We first calculate $U_S\left|\Psi_B^R\right\rangle$, $U_S\left|\Psi_B^G\right\rangle$, and $U_S\left|\Psi_B^B\right\rangle$ to get three $2^{n+3}\times 1$ vectors of using Matlab. Next, we obtain the vector of $U_S^C\left|\Psi_B^{24}\right\rangle$ using (39). We can apply U_S^C to a 64×64 color image by adopting the method, the simulation results of which are shown in Fig.19 and Fig.20.

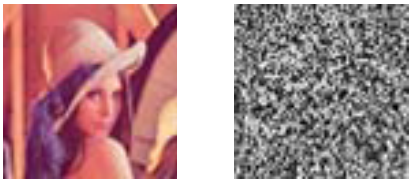

(a) (b)

FIGURE 19. A color image scrambling algorithm based on bitplanes. (a) a color image of 64 × 64. (b) The result of image scrambling.

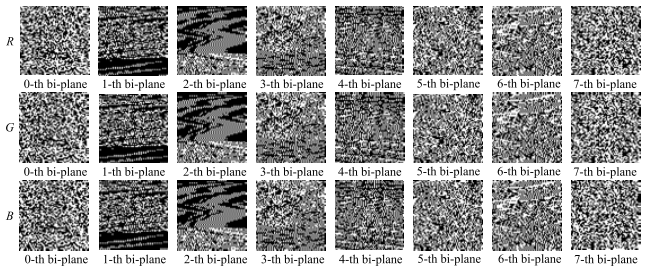

FIGURE 20. Bitplanes of the transformed images in Fig.19 (c).

F. COMPARISON ANALYSIS OF QUANTUM OPERATIONS FOR DIFFERENCE QIRS

Quantum cost (i.e., time complexity) is the key performance indicators of quantum operations, thus, we compare and analyze quantum costs of these operators in above for different QIRs. According to the method in [24] and [25], CNOT gate has a quantum implementation cost of 1, and its cost far exceeds the cost of NOT gate. Suppose that the cost of NOT gate is δ, we list the costs of some basic gates in Table 2.

For NEQR, INEQR, NCQI, and GNEQR, the complement of colors, reverse of bitplanes, and translation of bitplanes are implemented by the circuits in Fig.21. The circuits in (a), (b), and (c) implement the complement, reverse, and translation operations of grayscale images for NEQR, INEQR, and GNEQR. Furthermore, the circuits in (d), (e), and (f) implement the complement, reverse, and translation operations of RGB color images for NCQI and GNEQR. The pixel interchange operations of bitplanes (i.e., U_I and U_I^C) are difficult to be implemented by other QIRs.

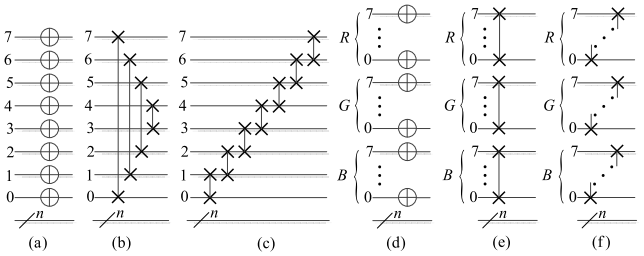

FIGURE 21. The complement of colors, reverse of bitplanes, and translation of bitplanes for NEQR, INEQR, NCQI, and GNEQR.

Next, quantum costs of these quantum operators for grayscale images (GI) or RGB color images (CI) are listed in Table 3.

TABLE 3. The costs of some basic gates.

Operation	NEQR	INEQR	NCQI	GNEQR	BRQI
Complement (GI)	$8\,\delta$	$8\,\delta$	-	$8\,\delta$	δ
Reverse (GI)	12	12	-	12	$3\,\delta$
Translation (GI)	21	21	-	21	$6+\delta\approx 6$
Complement (CI)	-	-	$24\,\delta$	$24\,\delta$	δ
Reverse (CI)	-	-	36	36	$3\,\delta$
Translation (CI)	-	-	63	63	$6+\delta\approx 6$
U_I and U_I^C	-	-	-	-	10
U_S and U_S^C	-	-	-	-	$16+5\delta\approx 1$

We can conclude that BRQI have lower quantum cost than other QIRs for some quantum operations based on bitplanes in Table 3.

Meanwhile, we can implement the algorithms of image scrambling for grayscale and color images by quantum circuits, quantum cost of which are only 16.

V. CONCLUSION AND FUTURE WORKS

In this article, we proposed a quantum image representation based on bitplanes (BRQI), which represent a grayscale and color image of 2^n pixels using $(n+4)$ and $(n+6)$ qubits, respectively. Compared with other QIRs, we concluded that the storage capacity of BRQI improves 16 times than NEQR, INEQR, and GNEQR for grayscale images, and improves 2^{18} times than NCQI and GNEQR for color images. Therefore, BRQI has displayed the enormous storage capacity. Furthermore, we designed the implementation circuits of BRQI and the method of simulation verification using Matlab.

Next, we presented some quantum operations based on BRQI, these operations including complement of colors, reverse of bitplanes, and translation of bitplanes. Analyzing their implementation circuits, we found that these operations based BRQI has lower quantum cost than ones based on other QIRs. Combining the above operations, we designed an algorithm of scrambling algorithm. Simulation results and performance analysis showed that the image scrambling algorithm is effective and efficient.

In conclusion, we consider that BRQI has significance for the devolvement of QuIP.

Our future works are how to design more complex algorithms based on BRQI.

REFERENCES

[1] M. A. Nielsen and I. L. Chuang, *Quantum Computation and Quantum Information*. Cambridge, U.K.: Cambridge Univ. Press, 2000.
[2] S. E. Venegas-Andraca and S. Bose, "Storing, processing, and retrieving an image using quantum mechanics," in *Proc. SPIE Conf. Quantum Inf. Comput.*, 2003, pp. 137–148.
[3] S. E. Venegas-Andraca and J. L. Ball, "Processing images in entangled quantum systems," *Quantum Inf. Process.*, vol. 9, no. 1, pp. 1–11, 2010.
[4] P. Q. Le, F. Dong, and K. Hirota, "A flexible representation of quantum images for polynomial preparation, image compression, and processing operations," *Quantum Inf. Process.*, vol. 10, no. 1, pp. 63–84, 2011.
[5] B. Sun, A. M. Iliyasu, F. Yan, F. Dong, and K. Hirota, "An RGB multi-channel representation for images on quantum computers," *J. Adv. Comput. Intell. Intell. Inform.*, vol. 17, no. 3, pp. 404–417, 2013.
[6] H. S. Li, Q. Zhu, S. Lan, C.-Y. Shen, R. Zhou, and J. Mo, "Image storage, retrieval, compression and segmentation in a quantum system," *Quantum Inf. Process.*, vol. 12, no. 6, pp. 2269–2290, 2013.
[7] H.-S. Li, Q. Zhu, R.-G. Zhou, L. Song, and X.-J. Yang, "Multi-dimensional color image storage and retrieval for a normal arbitrary quantum superposition state," *Quantum Inf. Process.*, vol. 13, no. 4, pp. 991–1011, 2014.
[8] H.-S. Li, Q. Zhu, M.-C. Li, and H. Ian, "Multidimensional color image storage, retrieval, and compression based on quantum amplitudes and phases," *Inf. Sci.*, vol. 273, pp. 212–232, Jul. 2014.
[9] R.-G. Zhou, Q. Wu, M.-Q. Zhang, and C.-Y. Shen, "Quantum image encryption and decryption algorithms based on quantum image geometric transformations," *Int. J. Theor. Phys.*, vol. 52, no. 6, pp. 1802–1817, 2013.
[10] F. Yan, A. M. Iliyasu, and S. E. Venegas-Andraca, "A survey of quantum image representations," *Quantum Inf. Process.*, vol. 15, no. 1, pp. 1–35, 2016.
[11] F. Yan, A. M. Iliyasu, and Z. Jiang, "Quantum computation-based image representation, processing operations and their applications," *Entropy*, vol. 16, no. 10, pp. 5290–5338, 2014.
[12] Y. Zhang, K. Lu, Y. Gao, and M. Wang, "NEQR: A novel enhanced quantum representation of digital images," *Quantum Inf. Process.*, vol. 12, no. 8, pp. 2833–2860, 2013.
[13] N. Jiang and L. Wang, "Quantum image scaling using nearest neighbor interpolation," *Quantum Inf. Process.*, vol. 14, no. 5, pp. 1559–1571, 2015.
[14] H. S. Li *et al.*, "Quantum implementation circuits of quantum signal representation and type conversion," *IEEE Trans. Circuits Syst. I, Reg. Papers*, to be published.
[15] J. Sang, S. Wang, and Q. Li, "A novel quantum representation of color digital images," *Quantum Inf. Process.*, vol. 16, no. 2, p. 42, 2017.
[16] H.-S. Li, P. Fan, H.-Y. Xia, S. Song, and X. He, "The multi-level and multi-dimensional quantum wavelet packet transforms," *Sci. Rep.*, vol. 8, Sep. 2018, Art. no. 13884.
[17] P. Fan, R.-G. Zhou, N. Jing, and H.-S. Li, "Geometric transformations of multidimensional color images based on NASS," *Inf. Sci.*, vols. 340–341, pp. 191–208, 2016.
[18] P. Botsinis, S. X. Ng, and L. Hanzo, "Quantum search algorithms, quantum wireless, and a low-complexity maximum likelihood iterative quantum multi-user detector design," *IEEE Access*, vol. 1, pp. 94–122, 2013.
[19] Y.-L. Gao, X.-B. Chen, Y.-L. Chen, Y. Sun, X.-X. Niu, Y.-X. Yang, "A secure cryptocurrency scheme based on post-quantum blockchain," *IEEE Access*, vol. 6, pp. 27205–27213, 2018.
[20] R.-G. Zhou, W. Hu, P. Fan, and G. Luo, "Quantum color image watermarking based on Arnold transformation and LSB steganography," *Int. J. Theor. Phys.*, vol. 16, no. 3, p. 1850021, 2018.
[21] N. Zhou, W. Chen, X. Yan, and Y. Wang, "Bit-level quantum color image encryption scheme with quantum cross-exchange operation and hyper-chaotic system," *Quantum Inf. Process*, vol. 17, p. 137, Jun. 2018.
[22] N. Jiang, L. Wang, and W.-Y. Wu, "Quantum Hilbert image scrambling," *Int. J. Theor. Phys.*, vol. 53, no. 7, pp. 2463–2484, 2014.
[23] R.-G. Zhou, Y.-J. Sun, and P. Fan, "Quantum image Gray-code and bit-plane scrambling," *Quantum Inf. Process.*, vol. 14, no. 5, pp. 1717–1734, 2015.
[24] J. A. Smolin and D. P. DiVincenzo, "Five two-bit quantum gates are sufficient to implement the quantum Fredkin gate," *Phys. Rev. A, Gen. Phys.*, vol. 53, no. 4, p. 2855, 1996.
[25] W. N. N. Hung, X. Song, G. Yang, J. Yang, and M. Perkowski, "Optimal synthesis of multiple output Boolean functions using a set of quantum gates by symbolic reachability analysis," *IEEE Trans. Comput.-Aided Design Integr. Circuits Syst.*, vol. 25, no. 9, pp. 1652–1663, Sep. 2006.

HAI-SHENG LI received the M.S. degree in computer science from Chongqing University in 2004 and the Ph.D. degree in computer science from the University of Electronic Science and Technology of China in 2014. He is currently an Associate Professor with Guangxi Normal University. His research interests include quantum information processing, quantum neural network, and image processing.

XIAO CHEN received the B.S. degree in electronics and information engineering from the University of Electronic Science and Technology of China (Chengdu College of University) in 2016. He is currently pursuing the master's degree with the Faculty of Electronic Engineering, Guangxi Normal University. His research interests include quantum information processing.

HAIYING XIA received the M.S. and Ph.D. degrees from the Department of Electronic and Information Engineering, Huazhong University of Science and Technology, Wuhan, China, in 2007 and 2011, respectively. She is currently an Associate Professor with Guangxi Normal University. Her current research interests include pattern recognition, medical image analysis, and neural networks.

YAN LIANG received the M.E. degree from the Guilin University of Electronic Technology in 2011. She is currently a Lecturer with Guangxi Normal University. Her research interests include signal processing and quantum information processing.

ZUOSHAN ZHOU received the M.S. degree from the Department of Transportation Engineering, Huazhong University of Science and Technology, Wuhan, China, in 2009. He was as a Lecturer with Guangxi Normal University. His research interests include e-commerce, town planning, and transport and logistics.